PCCP

PAPER

View Article Online
View Journal | View Issue

Cite this: *Phys. Chem. Chem. Phys.*, 2014, **16**, 10041

Microkinetics of oxygenate formation in the Fischer–Tropsch reaction†

Rutger A. van Santen,*[ab] Minhaj Ghouri[ab] and Emiel M. J. Hensen[a]

Received 22nd November 2013,
Accepted 29th January 2014

DOI: 10.1039/c3cp54950j

www.rsc.org/pccp

Microkinetics simulations are presented on the intrinsic activity and selectivity of the Fischer–Tropsch reaction with respect to the formation of long chain oxygenated hydrocarbons. Two different chain growth mechanisms are compared: the carbide chain growth mechanism and the CO insertion chain growth mechanism. The microkinetics simulations are based on quantum-chemical data on reaction rate parameters of the elementary reaction steps of the Fischer–Tropsch reaction available in the literature. Because the overall rate constant of chain growth remains too low the CO insertion chain growth mechanism is not found to produce higher hydrocarbons, except for ethylene and acetaldehyde or the corresponding hydrogenated products. According to the carbide mechanism available quantum-chemical data are consistent with high selectivity to long chain oxygenated hydrocarbon production at low temperature. The anomalous initial increase with temperature of the chain growth parameter observed under such conditions is reproduced. It arises from the competition between the apparent rate of C–O bond activation to produce "CH_x" monomers to be inserted into the growing hydrocarbon chain and the rate of chain growth termination. The microkinetics simulations data enable analysis of selectivity changes as a function of critical elementary reaction rates such as the rate of activation of the C–O bond of CO, the insertion rate of CO into the growing hydrocarbon chain or the rate constant of methane formation. Simulations show that changes in catalyst site reactivity affect elementary reaction steps differently. This has opposing consequences for oxygenate production selectivity, so an optimizing compromise has to be found. The simulation results are found to be consistent with most experimental data available today. It is concluded that Fischer–Tropsch type catalysis has limited scope to produce long chain oxygenates with high yield, but there is an opportunity to improve the yield of C_2 oxygenates.

1. Introduction

In addition to hydrocarbons the Fischer–Tropsch reaction, which is an important conversion step in the overall process that converts coal or natural gas into liquid hydrocarbon fuels, can also produce oxygenates.[1–3] The selectivity towards their formation strongly depends on reaction conditions as well as the catalytic material used. To produce oxygen containing hydrocarbons from synthesis gas (a mixture of CO and H_2) instead of by selective oxidation of the corresponding hydrocarbons may have advantages in terms of raw materials used or processing requirements. In heterogeneous catalysis the oxygenated long-chain hydrocarbon product can be formed through two essentially different reaction processes that are excellently reviewed in ref. 4 and 5.

CO can be initially hydrogenated to methanol and the methanol undergoes aldol type reactions that lead to a mixture of branched alcohols. The main investigated catalysts for this process are modified methanol catalysts, based on Cu, promoted by ZnO, Cr_2O_3 or additional additives to catalyze formation of higher alcohol oligomers.[6]

Alternative catalyst systems to be considered here are based on the Fischer–Tropsch reaction. In this reaction instead of becoming hydrogenated CO initially decomposes into an adsorbed "CH_x" intermediate that initiates an oligomerisation reaction. Oxygenate formation arises from the insertion reaction of CO in the growing adsorbed hydrocarbon chain. A transition metal component of such catalysts, that has been extensively studied, is Rh.[7,8]

We will present results of microkinetics simulations that address the improvement of selectivity of oxygenate formation *versus* that of hydrocarbon formation, which is a key issue with respect to the application of this catalytic system.

In order to study the microkinetics of this reaction two main competitive mechanistic proposals for the hydrocarbon chain growth reaction have to be considered.[9] The most generally

[a] *Laboratory of Inorganic Materials Chemistry, Department of Chemical Engineering and Chemistry, Eindhoven University of Technology, PO Box 513, 5600MB, Eindhoven, The Netherlands. E-mail: r.a.v.santen@tue.nl*
[b] *Institute for Complex Molecular Systems, Eindhoven University of Technology, PO Box 513, 5600MB, Eindhoven, The Netherlands*

† Electronic supplementary information (ESI) available. See DOI: 10.1039/c3cp54950j

accepted is the carbide mechanism.[10] According to this mechanism chain growth occurs by consecutive insertion of CH_x intermediates. This is different from the alternative proposal, originally by Pichler and Schulz[11] that proposes hydrocarbon growth through CO molecule insertion into the growing hydrocarbon chain. There is no consensus on which of the two mechanisms is preferred. For a recent analysis we refer to the literature.[12,13] To decide between the two mechanistic options of chain growth is practically important because it provides different criteria for catalyst composition and structure choices to optimize CO conversion rates and product selectivity.

We will compare these criteria with experimental information as mainly summarized in the two review papers.[4,5]

All of the known Fischer–Tropsch catalysts produce oxygenates, but with widely varying selectivities, which not only depend on the catalyst material, but also strongly on reaction conditions.[14]

Important additional questions with respect to the optimization of the catalyst relate to structure dependence, the role of promoters and the use of alloys.

The microkinetics simulations to be presented are based on consideration of the complete set of elementary reaction steps leading to such products. An earlier study also based on such an approach was reported by Storsaeter *et al.*[15] Since several elementary reaction steps compete, the microkinetics simulations will have to be solved without making *a priori* assumptions on rate controlling steps. For this reason the ordinary differential equations that follow from the kinetics schemes used will be solved directly using the ordinary differential equations (ODE) suite which comes with the software program Matlab©.

The simulation strategy is similar to that we used in previous papers,[12,13] which however only considered hydrocarbon formation and did not include oxygenate formation as will be done here.

The experimental distribution of Fischer–Tropsch hydrocarbon chains shows an approximately ASF (Anderson–Schulz–Flory) distribution.[3,16] When the product distribution is plotted as a function of hydrocarbon chain length an exponential distribution is found. This implies that the chain growth rate is independent of hydrocarbon chain length beyond a particular chain length that is typically for C_3 and higher chain length. The slope of this distribution plot gives chain growth probability α (see also eqn (1)). We have also used this property in the simulations by assuming the microkinetics chain growth parameters to be independent of chain length.

The molecular data on reaction intermediates and activation energies of elementary reaction steps will be based on published quantum-chemical data, which we have extensively reviewed elsewhere for the carbide mechanism[12,13] and for the CO insertion chain growth mechanism in ref. 21. The input data used can be considered representative of Co, Ru or Rh metal surfaces with different structures. For consistency the microkinetics elementary reaction rate data have been adapted to confirm with the overall thermodynamics of the relevant Fischer–Tropsch products.

Different surface topologies change significantly the relative rate constants of CO activation *versus* that of methane formation, chain growth termination and C–C bond formation.

In the case of the chain growth reaction through CO insertion proposed by Cheng *et al.*[17] for stepped and non-stepped Co (0001) surfaces and in a later paper we demonstrated that most of the additional published quantum-chemical data lead to the conclusion that this reaction mechanism can be excluded.[13,21] However recently an interesting paper by Saeys *et al.*[18] appeared that demonstrated a high sensitivity of key activation energy parameters to surface coverage. Of special interest is their suggestion that at high coverage lateral effects decrease the activation barriers for CO insertion into the growing hydrocarbon chain substantially, which would favour high chain growth according to this reaction route. This is important because simulations indicate[12] that long chain hydrocarbon selectivity is consistent with a high coverage of CO. For this reason we took the high surface coverage reaction energy data of Saeys *et al.*[18] calculated for the Co(0001) surface as the default values for the CO insertion chain growth reaction.

In the microkinetics simulations to be presented here we will calculate selectivity and CO conversion rates under practical conditions. We will be interested in catalyst performance changes as a consequence of different choices of rate parameters that reflect catalyst composition as well as structure.

It will appear that selectivity to long chain oxygenate formation depends on the balance of several elementary rate constants that sometimes counteract. In the discussion and conclusion section the optimum microkinetics relations between elementary rate constants will be discussed. Through quantum-chemistry this can be related to composition and catalyst structure requirements, which provide a basis to compare theory with experiment in the Conclusion: comparison of theory and experiment section.

2. Method

Microkinetics model descriptions including the mechanistic schemes in terms of the complete set of elementary reactions and their corresponding rate parameters for both the carbide chain growth mechanism as well as CO insertion mechanism studied in this report are presented in this section.

2.1 Carbide chain growth mechanism

Fig. 1 shows a schematic presentation of the kinetic model according to the carbide chain growth model explored in the present work. Mechanistic pathways leading to the formation of up to C_3 olefin and oxygenates can be seen in the figure. Based on previous work[13,19] the CH_{ads} monomer is considered as the building block that gets incorporated into the growing chain. The chain growth pathways are green color coded in the figure. Oxygenate termination pathways *via* a CO insertion step are represented in yellow and elementary steps leading to the termination of olefins are shown in blue. The CH_{ads} monomer, which is formed by the hydrogenation of carbon from the

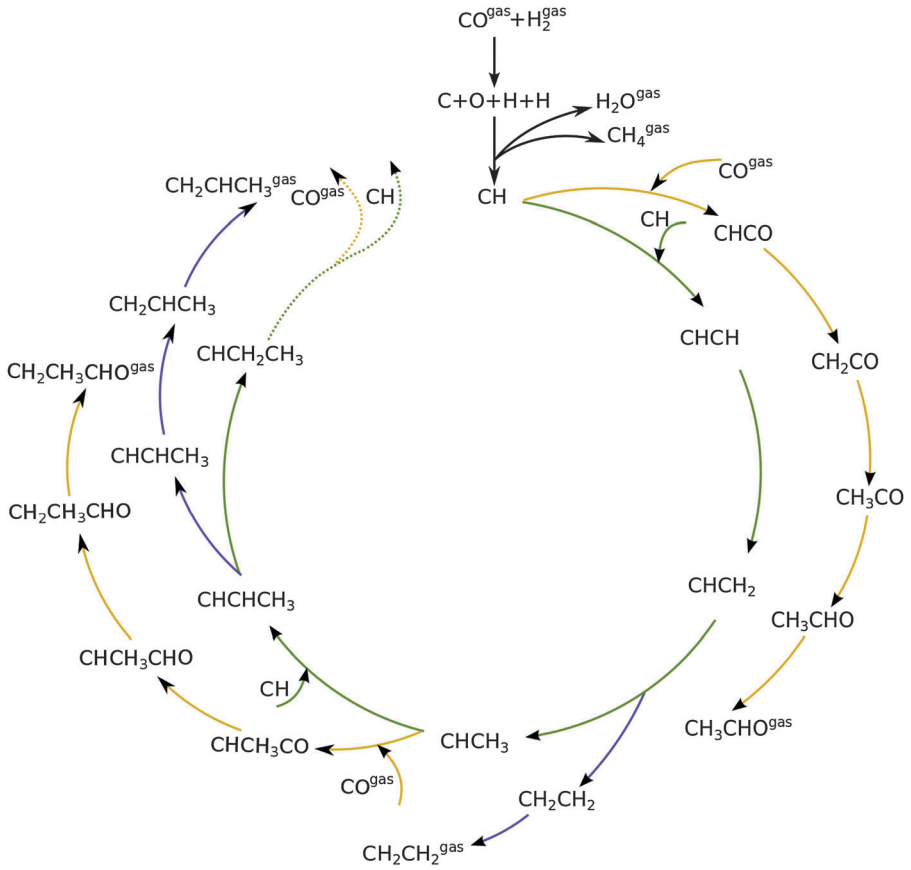

Fig. 1 The mechanistic scheme for the Fischer–Tropsch reaction implemented for the formation of olefins as well as oxygenates. When the reaction intermediate does not have the "gas" label it is considered to be chemisorbed.

directly dissociated CO, is considered to be the building block for subsequent chain growth.

There are three prerogatives for the initial CH_{ads} monomer. It can undergo further hydrogenation steps desorbing as methane. Another path for it is the coupling with CO to form CHCO. This species further goes through three hydrogenation steps to terminate as acetaldehyde. The final option for the CH_{ads} monomer is to couple with another CH_{ads} species leading to the pathway towards chain growth. This CHCH species on the surface can now go through a hydrogenation step to form $CHCH_2$. Further addition of a hydrogen atom to the primary carbon leads to the termination of the chain as an olefin, ethylene in this case. Addition of the hydrogen atom to the secondary carbon atom leads it towards further chain growth. This alkylidene type of chain can either terminate into a corresponding aldehyde by going through CO insertion and subsequent hydrogenation steps; recombination of this with CH leads to either its termination into an olefin or towards further chain growth. The work presented here includes the formation of olefins and oxygenates up to a chain length of C_{50}.

As discussed elsewhere, another important technical aspect of first principle microkinetics simulations is that simulations are to be done including production of hydrocarbon chains of sufficient length so as to prevent spurious cut-off effects that result from reversibility of all the chain growth reactions included.[20] The chain growth parameter α for oxygenate formation and alkane formation has to be the same, which can be used as a test criterion for convergence of the simulations.

Fig. 2 shows the relative adsorption energies and the activation barriers for various intermediates leading to the formation of propionaldehyde. Based on available quantum chemical data we have constructed the energy profiles of this reaction. Formation of all longer hydrocarbons as well as oxygenates is considered to be homologous and proceeds through insertion of a CH species in agreement with the chain growth model proposed before for Ru.[19] CH_{ads} is the monomer that is incorporated into the growing adsorbed hydrocarbon chain. This mechanism corresponds to the generally accepted carbide mechanism in which CH_x species is the surface species to be inserted into the growing hydrocarbon chain. The reaction energy diagrams of all higher carbon number products (hydrocarbons as well as oxygenates) have similar elementary reaction rate parameters, so that the product distribution may be expected to correspond to the logarithmic ASF distribution with chain growth parameter α independent of the chain length.

Activation entropies have been chosen to be different from zero only for reactions between the gas phase and the solid. Further details about the actual prefactors used and their calculation details can be found in the ESI† accompanying this article. Readsorption from the gas phase is ignored in the simulations.

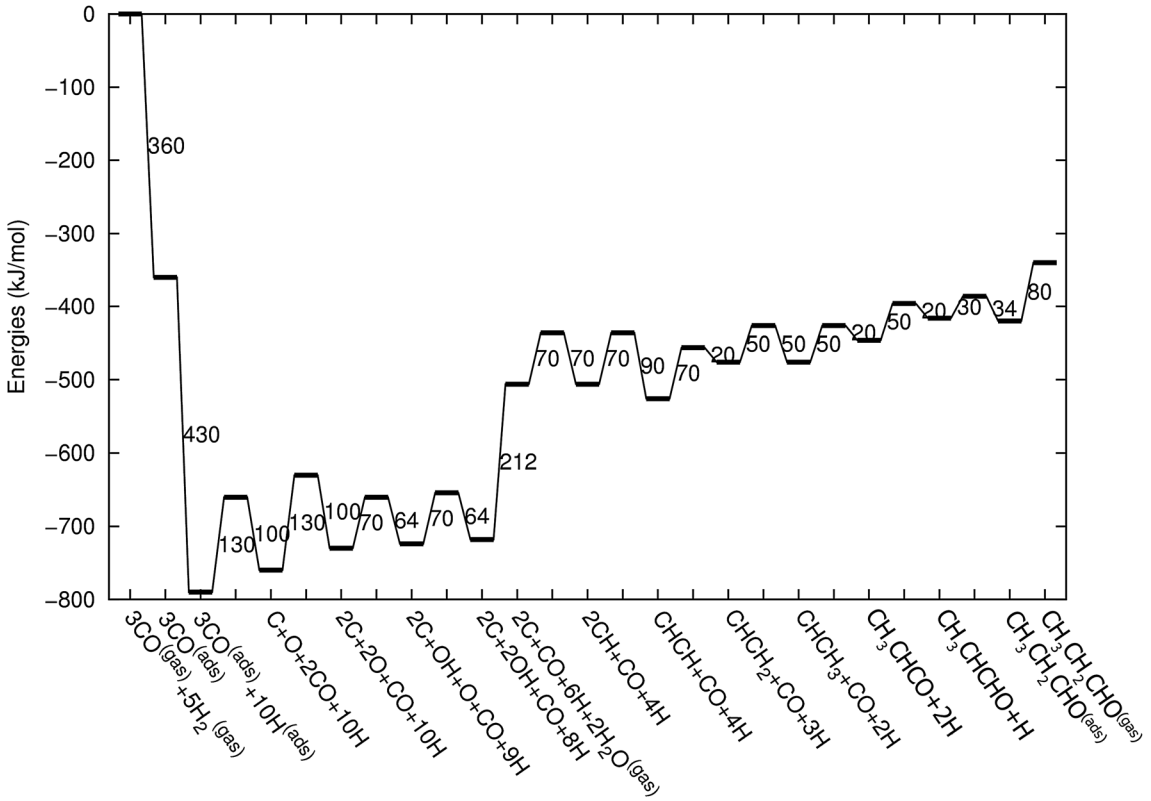

Fig. 2 The reaction energy diagram, with default values of activation energies and reaction energies for the formation of propionaldehyde as a function of progress of the reaction. Reaction intermediate energies and relative stabilities with respect to the gas phase are given. For additional details we refer to ESI.†

The rate constants used in the microkinetics schemes are based on activation energies available from recent DFT quantum-chemical calculations reviewed in ref. 21. Activation energies of elementary reaction rate constants and relative energies of surface intermediates will depend on surface structure as well as catalyst composition. In the simulations we have selected default values that are representative for reactive Co or Ru surfaces. Variation of parameters as the activation energies of the CO dissociation reaction or the CH_{ads} to methane transformation reaction represent different choices of surface or composition.

Quantum-chemical data based on DFT computations cannot be expected to be more accurate than 10 kJ mol^{-1}. For this reason absolute values of predicted elementary reaction rates in comparison to experiment may be expected to have a significant error. In microkinetics studies the systematic errors that lead to the inaccuracies of the quantum-chemical calculations lead sometimes to approximate cancellations, which reduces the error in predicted temperature maxima in such simulations. So may errors in energies of adsorption cancel errors in activation energies.

In the comparative kinetic studies considered here we have maintained most of the reaction energy data invariant, but have changed reaction rate data of elementary reaction steps of interest by altering the activation energies substantially more than 10 kJ mol^{-1}. The results obtained should be considered qualitative in an absolute sense, but reliable in a comparative sense.

Fig. 3 shows the energy diagrams for the production of propylene as well as higher olefins when the oxygenate products are included in the model and when there is no oxygenate production. An important reference to the quantum-chemical data is Kapur *et al.*[22] For a review we refer to Van Santen *et al.*[21]

The energy diagram when no oxygenates are produced is the same as used earlier.[12,13] As in previous simulations we have chosen H_2O formation to be a relatively fast reaction.

2.2. CO insertion chain growth mechanism

In Fig. 4 the two reaction mechanistic schemes studied for the CO insertion chain growth mechanism are shown. They differ by a choice of which oxygen containing surface intermediate cleaves its bond. In scheme (a) the C–O bond cleaves in the CH_3CO species, in scheme (b) this occurs in the aldehyde molecule. Which of the two steps occur determines the competitive reaction steps with chain growth. While in case (a) rapid hydrogenation of CH_3CO would cause interference with a high chain growth rate, in case (b) this would be the desorption of aldehyde. The corresponding reaction diagrams shown in Fig. 5 and 6 have been constructed using the high coverage data of Saeys and co-workers on Co(0001).[18] Since their data are not complete and do not close the catalytic reaction cycle we have used representative data from available literature.[12,21]

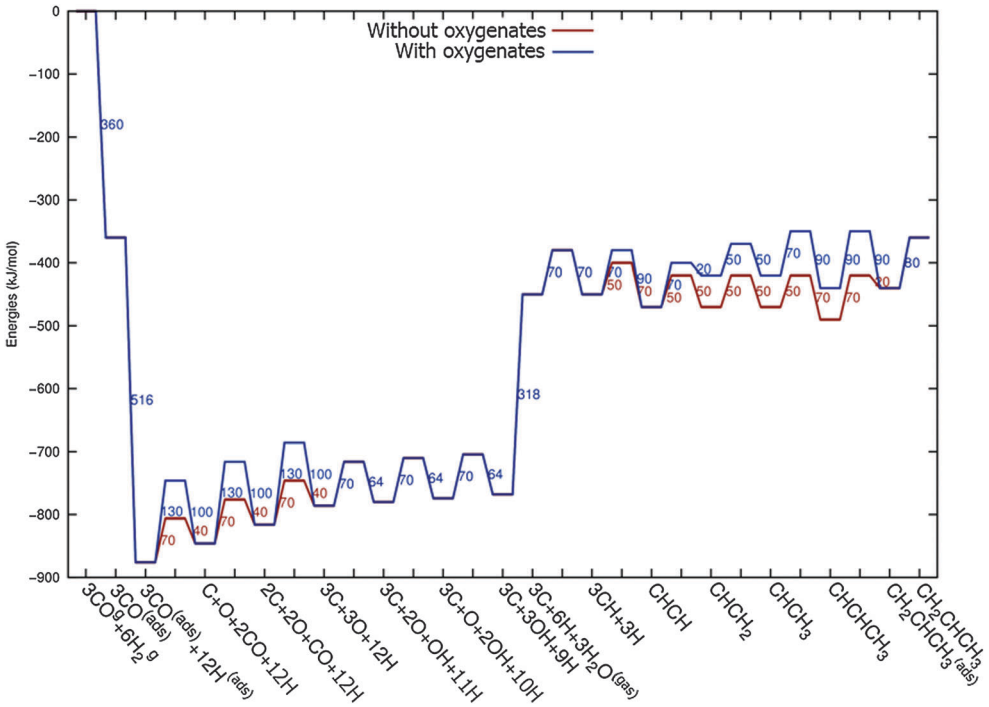

Fig. 3 The reaction energy diagram for the formation of propylene when the product selectivity is biased towards the production of oxygenates (blue line) and when the oxygenates are not included in the model (red line). Default values for (activation) energies are used in the diagram. Energies are given with respect to the gas phase. For additional details we refer to ESI.†

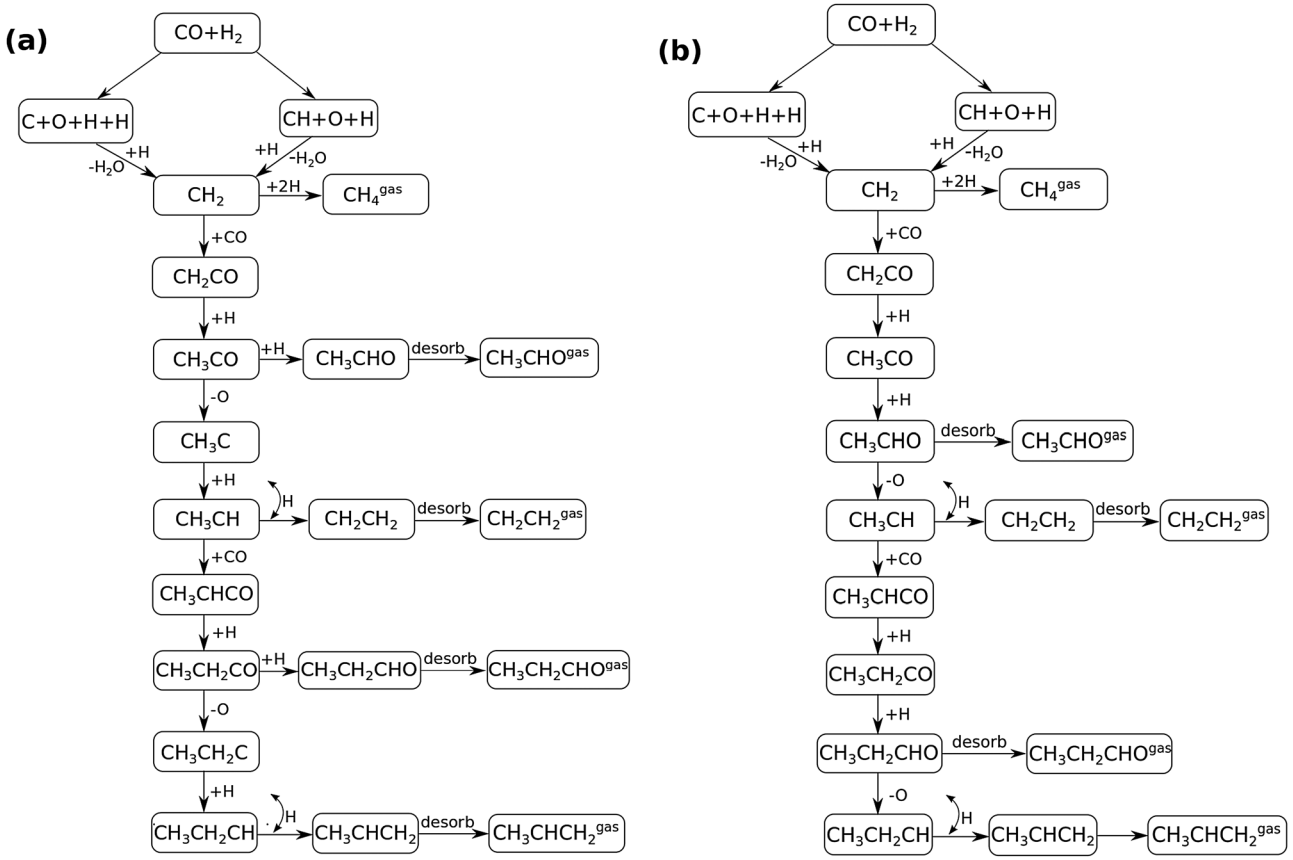

Fig. 4 Fischer–Tropsch reaction mechanistic schemes used in the microkinetics simulations to model the chain growth *via* CO insertion. The difference in the schemes (a) and (b) is in the C–O bond scission step. In scheme (a) C–O bond cleavage takes place before the formation of surface aldehyde, whereas in scheme (b) the C–O bond cleaves after the formation of surface aldehyde and before it desorbs from the surface.

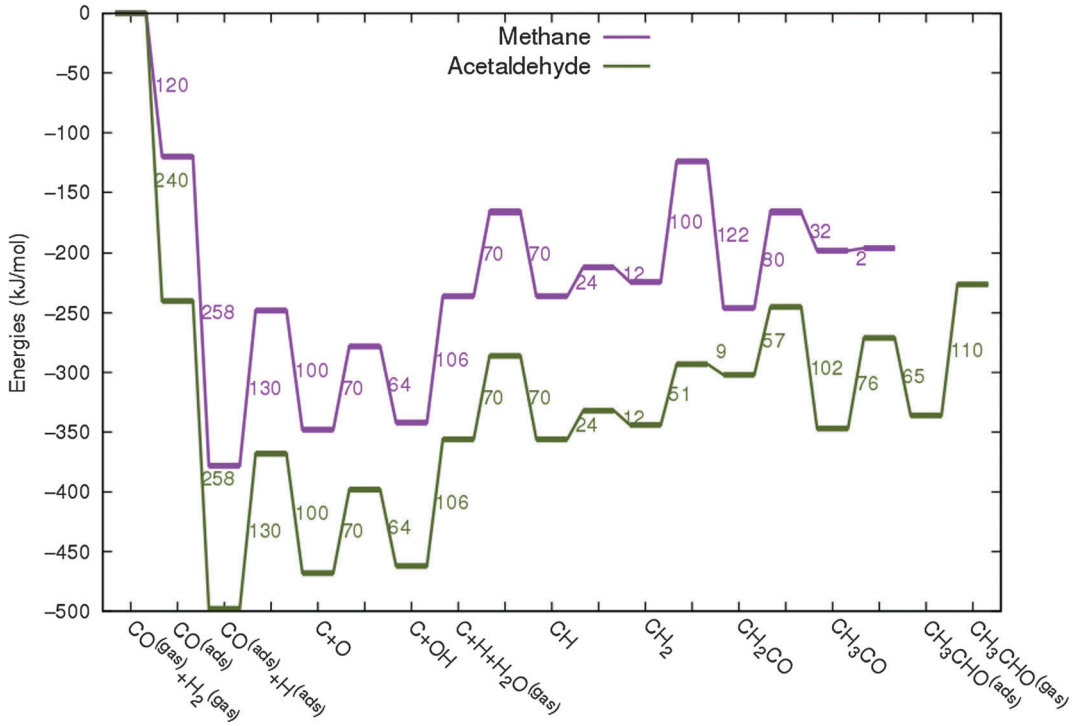

Fig. 5 The reaction energy diagram for the formation of methane and acetaldehyde *via* the CO insertion chain growth model. The formyl route of CO activation leading to CH species from CO is included in the simulations but is not implied here. Higher oxygenates formation is homologous to the rate of formation of acetaldehyde. The last steps in methane formation reaction energy diagram concern $CH_{3,ads}$ and $CH_{4,ads}$ formation. Part of the reaction energies data is adapted from Saeys *et al.*[18] Default values for (activation) energies have been used. Energies are given with respect to the gas phase. For additional information we refer to ESI.†

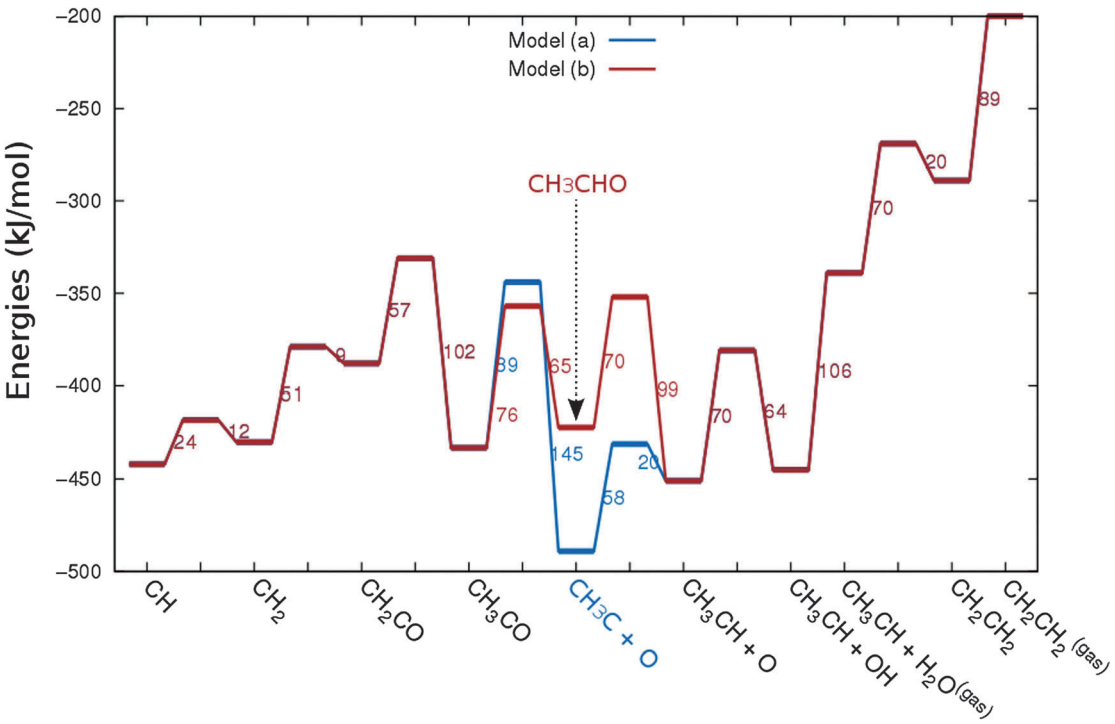

Fig. 6 The reaction energy diagram for the formation of ethylene *via* the CO insertion chain growth mechanism. Higher olefin formation is homologous to the rate of formation of ethylene. This energy diagram corresponds to the scheme shown in Fig. 4(a) and (b). Reaction energies data are adapted from Saeys *et al.*[18] Default values for the (activation) energies have been used. Energies are given with respect to the gas phase. For additional information we refer to ESI.†

3. Results and discussion

The results to be presented enable us to address the relative importance of the hydrogen activated CO *versus* the path of C–O bond cleavage through direct CO activation and the validity of the different mechanistic proposals of the formation of oxygenated higher hydrocarbons.

We will analyze in Section 3.1 oxygenate formation according to the carbide mechanism and in Section 3.2 oxygenate and olefin formation according to the CO insertion chain growth mechanism.

The issue of hydrogen activated C–O bond cleavage[23–27] is especially relevant to the carbide mechanism of the Fischer–Tropsch reaction and will be discussed in Section 3.1.1. In the carbide chain growth mechanism chain growth proceeds by intermediate formation of "CH" that we identified previously as the monomer species inserted into the growing hydrocarbon chain.[13]

As we have reviewed elsewhere[12,28] Fischer–Tropsch catalysis using transition metals such as Ru[29] or Co,[30,31] or oxygenate production on Rh[32,33] is strongly particle size dependent. The CO consumption rate and chain growth parameter α steeply decrease when transition metal particle sizes decrease below a few nanometers. This can be ascribed to the requirement of step-edge type sites, which are not present on the small particles.[61]

The step-edge sites provide low barriers for CO activation, reduce the rate of methane formation and chain growth termination.

In the simulations to be presented CO activation barriers as well as hydrogenation barriers of CH_x formation have been varied to simulate changes in surface structure of the catalysts and to provide a prediction of optimum site structure. The choice of metal tunes such effects. Activation barriers for C–O bond cleavage will be higher on Co or Rh than Ru,[34] whereas the M–C bond strengths tend to be stronger on Ru than Rh or Co[34] and hence the relative chain growth termination and methanation elementary rate constants. On the same surface site the activation energy of C–O bond activation on Rh is lower than that of Co, which makes Rh a more attractive catalyst material for oxygenate formation.[35]

Microkinetics simulations are indispensable because of the sometimes counteracting effects of reaction parameter changes when site structure or composition changes.

3.1 Oxygenate formation according to the carbide chain growth mechanism

3.1.1 Formyl *vs.* the direct path of CO activation. Fischer–Tropsch synthesis originates at the activation step of CO to give the C_1 monomer which incorporates itself into the growing chain. The mechanism of CO dissociation has important kinetic consequences on the overall rate of FT reaction. Two mechanisms which are discussed in the literature[9,24,36,37] are (i) direct dissociation of CO_{ads} to give surface species C_{ads} and O_{ads} and (ii) the formyl path of CO activation where adsorbed hydrogen reacts with adsorbed CO to give an unstable COH or HCO type of species which readily dissociates to give CH_{ads} and O_{ads}.

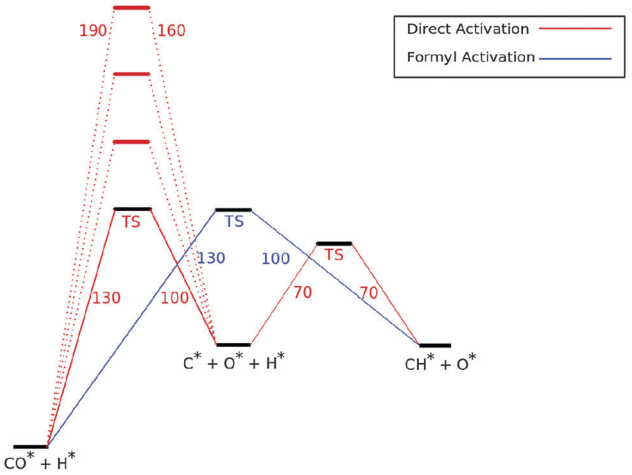

Fig. 7 The reaction mechanistic scheme and reaction barriers used to investigate the competition of direct *vs.* hydrogen assisted or the formyl path of CO dissociation. The mechanism until CH_{ads} formation is only shown. Numbers shown are respective barriers in kJ mol^{-1}. In red the activation barriers of the direct CO dissociation path are given. The high barriers of CO dissociation refer to surface terrace sites. The second barrier of the direct CO dissociation path concerns C_{ads} to CH_{ads} transformation. The black curve denotes the hydrogen activated CO dissociation reaction energy path. The transition state energy is that for the overall reaction energy of formyl intermediate formation and consecutive C=O bond cleavage.

Here we have employed microkinetics simulations to investigate the role of the formyl path of CO activation in the overall reaction rate of the FT reaction.

Fig. 7 shows the reaction energy diagram of the kinetic model constructed which includes both the direct and the hydrogen assisted paths of CO dissociation. The reaction schemes of direct CO dissociation and hydrogen activated C–O bond cleavage are based on calculations of Ru.[26,27,38,39] In the simulations to be presented the activation energy of direct CO activation will be varied with respect to that of the hydrogen activated case.

Earlier we argued[26] that in contrast to direct CO activation, the C–O bond cleavage path through intermediate CHO formation is relatively surface structure independent. On the dense Ru(0001) surface the corresponding low barrier of CH formation will make this route the preferred one,[27] but on reactive step-edge sites direct CO activation will become the preferred elementary reaction.

When there is direct CO dissociation, the CH_{ads} surface species is formed in two steps: CO dissociation to give C_{ads} and O_{ads} and the subsequent hydrogenation of C to give CH_{ads} (red lines in Fig. 7). In the hydrogen activated CO dissociation path CH_{ads} is the direct product. Transformation of CO_{ads} to CH_{ads} takes place through intermediate formyl formation and subsequent C=O bond cleavage. In Fig. 7 and the simulations the two relevant transition states and relative energy of the formyl intermediate have been taken together into a single transition state.

Calculated chain growth probability α and Turnover Frequencies (TOFs) for olefin and oxygenate yield are compared in Fig. 8 for the two models when CO activation only goes through direct

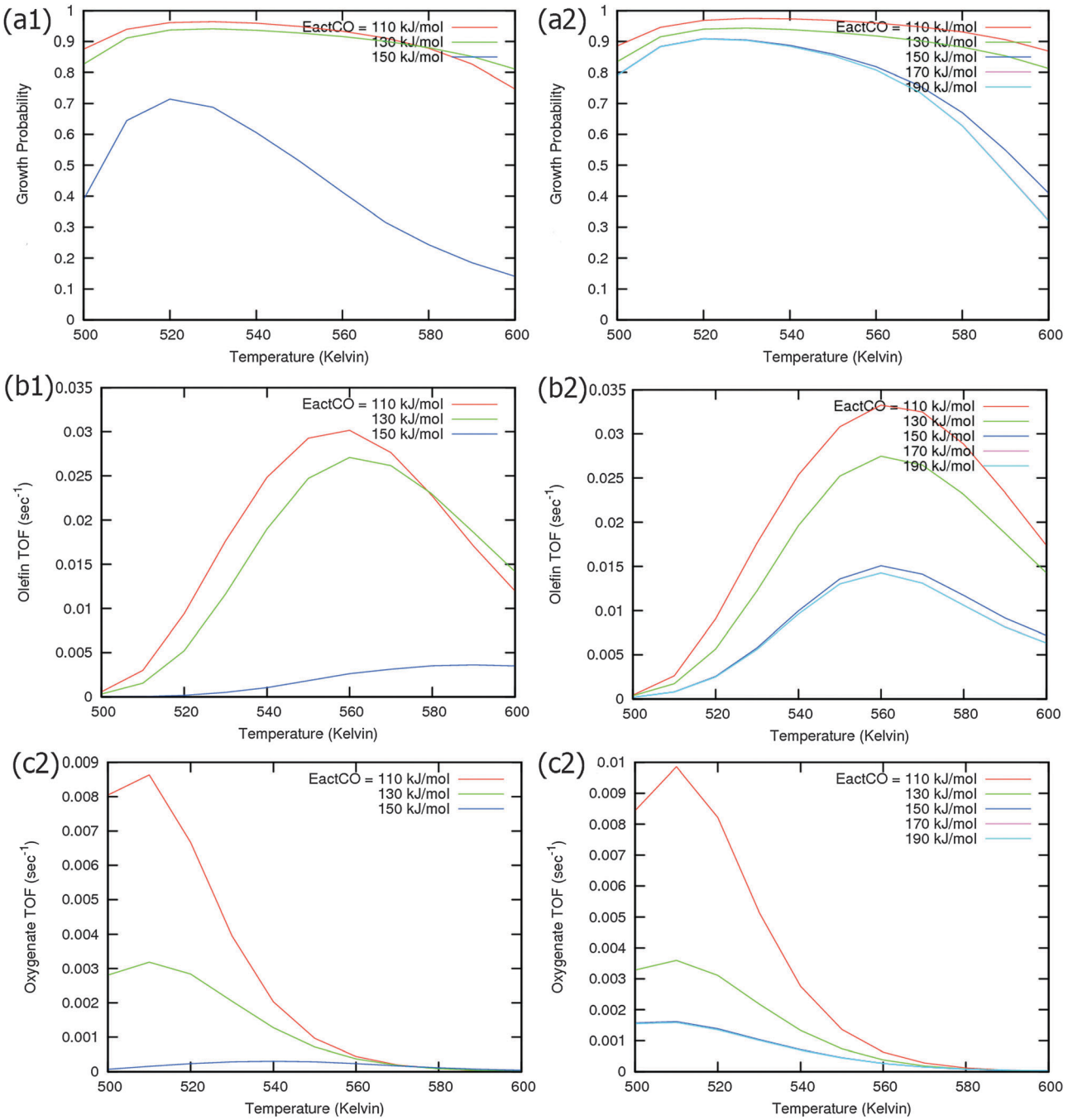

Fig. 8 Microkinetics simulations in competition between direct and hydrogen activated C–O bond cleavage. CO gas pressure is p_{CO} = 0.5 MPa and the H_2 gas pressure is P_{H_2} = 1.5 MPa. (a) Chain growth probability (α), (b) olefin TOF (s^{-1}) and (c) oxygenate TOF (s^{-1}) are compared when there is (1) no formyl path of CO activation (left) and when (2) the formyl path is included (right).

dissociation (Fig. 8(a1), (b1), and (c1)) and when the formyl path of CO activation is included in the simulation (Fig. 8(a2), (b2), and (c2)). The activation barrier for direct CO dissociation is varied within a range from 110 kJ mol^{-1} to 170 kJ mol^{-1} while keeping the formyl path barrier constant at 130 kJ mol^{-1}. The thermodynamics between these two competing pathways is the same and is endothermic by 30 kJ mol^{-1}.

Fig. 8a and b compare simulated chain growth parameters α, rates of C_2^+ olefin and the rate of C_2^+ oxygenate formation as a function of temperature. The rates of product formation are normalized per unit "C" consumed.

In Fig. 8a we observe a steep decrease in α and C_2^+ yield when the activation energy of direct CO activation exceeds 130 kJ mol^{-1}, whereas in Fig. 8b this decrease is absent since hydrogen activated C–O bond cleavage is included, which remains fixed at the overall activation energy of 130 kJ mol^{-1}.

At the lower activation energies, representative of CO activation on step-edge sites, we observe a high chain growth as well

as a high CO consumption rate. At the higher activation energies of CO it starts to compete with hydrogen activated CO dissociation, which then becomes dominating. Then with our chosen parameters chain growth parameter α initially remains relatively high, but decreases steeply with temperature when total C_2^+ yield becomes maximum.

Initially at low temperature the selectivity towards oxygenate formation exceeds that of hydrocarbon formation, but this selectivity rapidly declines with temperature. The latter is due to the high activation barrier of CO insertion compared to the activation energy of alkene chain growth termination.

The dominating production of oxygenates at low temperature, and decrease of oxygenate selectivity with temperature is in agreement with experimental observations on nanoparticles of Ru.[40]

Of interest also is the agreement between these experimental results and the anomalous initial increase in chain growth parameter α with temperature. Whereas usually chain growth parameter α decreases with temperature we observe in the simulations that it increases with temperature, when low temperature oxygenate formation is also included.

This maximum in the α value as a function of temperature is due to the need to dissociate the C–O bond to form the "CH" intermediate that is to be inserted into the growing hydrocarbon chain. This unique behavior of chain growth parameter α is nicely illustrated by consideration of the course grained kinetics expressions for α that one deduces for the case of only oxygenate formation (eqn (5)) *versus* that for alkene formation (eqn (4)). They follow from the general lumped kinetics expression for α:[9]

$$\alpha = \frac{k(n,n-1)\theta_{c_1}}{k(n,n-1)\theta_{c_1} + k_t^O + k_t^H} \quad (1)$$

In eqn (1), $k(n, n-1)$ is the lumped kinetics rate constant of "C_1" insertion into the growing hydrocarbon chain, θ_{c_1}, the surface concentration of "C_1" and k_t^O and k_t^H the respective lumped kinetics rate constants of chain growth termination to give the oxygenate or hydrocarbon. As eqn (2) indicates k_t^O is proportional to θ_{CO}, the surface coverage of CO is:

$$k_t^O = k_t' \theta_{CO} \quad (2)$$

As we have shown previously,[12] an elegant expression can be deduced for θ_{c_1}, when the transformation rate of adsorbed CO to "C_1", k_{CO}^{diss} controls the rate of CO consumption. This is the Fischer–Tropsch monomer formation kinetics limit, which applies to most of the practical catalysts. With the chosen activation energy for CO activation in this section this limit also applies to the low temperature simulations.

$$\theta_{c_1} = \left[\frac{(k_t^O + k_t^H)k_{CO}^{diss}\theta_{CO}(1-\theta_{CO})}{\left(k_{(n,n-1)}\right)^2}\right]^{1/3} \quad (3)$$

When one substitutes expressions eqn (2) and (3) into expression eqn (1) one deduces two different limiting expressions for α. One finds in case oxygenate formation dominates eqn (4) and for only hydrocarbon formation eqn (5).

$$\alpha^0 = \left(1 + \left(\frac{k_t'^2\theta_{CO}}{k(n,n-1)k_{CO}^{diss}(1-\theta_{CO})}\right)^{1/3}\right)^{-1} \quad (4a)$$

$$= \left(1 + \left(\frac{k_t'^2\theta_{CO}}{k(n,n-1)k_{CO}^{diss}}K_{ads}p_{CO}\right)^{1/3}\right)^{-1} \quad (4b)$$

$$\alpha^H = \left(1 + \left(\frac{k_t^2}{k(n,n-1)k_{CO}^{diss}\theta_{CO}(1-\theta_{CO})}\right)^{1/3}\right)^{-1} \quad (5a)$$

$$= \left(1 + \left(\frac{k_t^2(1+K_{ads}p_{CO})^2}{k(n,n-1)k_{CO}^{diss}K_{ads}p_{CO}}\right)^{1/3}\right)^{-1} \quad (5b)$$

In eqn (4b) and (5b) K_{ads} is the equilibrium constant of CO adsorption and p_{CO} the CO partial pressure.

The low initial value of α at low temperature may arise when surface vacancies have to be created for CO dissociation. However, when the activation energy of the termination reactions is high, this will dominate the temperature dependence and α shows regular behaviour and decreases with temperature. The mathematical condition for the occurrence of a maximum in α with temperature is given by:

$$E_{act}^{CO} + E_{ads}^{CO} > 2\bar{E}_t - E_{n,n-1} \ (\theta_{CO} \approx 1) \quad (6)$$

Eqn (6) applies exactly to the case of eqn (4) and to the case of eqn (5) in the high pressure limit. $\bar{E}_t$ denotes the respective activation energies for chain growth termination and $E_{n,n-1}$ the activation energy of the chain growth rate constant.

The sum of activation energy of CO dissociation and adsorption energy of CO (E_{ads}^{CO}), that defines the apparent activation energy of a CO covered surface, has to be relatively large and the activation energy of the termination reactions should not be too high.

As can be readily verified from the parameter choices presented in Section 2, eqn (6) will be usually satisfied. The anomalous temperature dependence of α can be expected at low temperatures when the selectivity towards oxygenate formation dominates. The selectivity of oxygenate formation decreases with temperature since the apparent activation energy of k_t^O strongly increases with decreasing θ_{CO} so that the rate constant of oxygenate formation is overtaken by the rate constant of olefin termination. The physical reason for the appearance of the temperature maximum in α is that at low temperature the surface is blocked by the high coverage with adsorbed CO. Once surface vacancies arise due to CO desorption, CO dissociation occurs and chain growth begins. As is especially seen in Fig. 8(a1) the maximum becomes more pronounced when the activation energy for CO dissociation increases.

Because of the very small additional effect on reaction yield of the inclusion of hydrogen activated C–O bond cleavage we take in the simulations that follow only the direct CO

dissociation path into account and use a default value of 130 kJ mol^{-1}. This activation barrier of CO activation is representative of the activation barrier of CO on stepped Co or Ru surfaces of intermediate reactivity,[9] with not too high activation barrier of CO so that oxygenate formation will occur.

3.1.2 CO partial pressure dependence. Fig. 9 shows the CO partial pressure dependence as well as CO coverage for the case of only direct CO activation with an activation energy of 130 kJ mol^{-1}.

One notes again the very different dependence of oxygenate and hydrocarbon yields as a function of temperature and in addition a very different CO partial pressure dependence. Fig. 9a indicates that at very low temperature oxygenate yield is low and decreases with increasing partial pressure of CO. This is because CO dissociation is inhibited by the increased CO pressure. However at the higher temperatures the oxygenate yield increases and shows a maximum at the lower of the additional temperatures used. At the higher temperature hydrocarbon formation takes over. At these temperatures the C_2^+ yield of oxygenates has a positive order in CO pressure. The CO coverages have substantially decreased (see Fig. 9c), the positive order in partial pressure of CO arises to maintain a finite rate of the CO insertion termination reaction. At the temperatures selected in Fig. 9b one observes a uniform increase in C_2^+ yield of hydrocarbons and the expected decrease in C_2^+ yield as a function of CO partial pressure for olefin formation.

One notes from the surface coverages shown in Table 1 that adsorbed CO is replaced by adsorbed "C_2" intermediates when the temperature increases. The increasing rate of CO consumption with temperature reduces the surface coverage with CO. The temperature maxima in yields of oxygenate formation correspond to a CO surface coverage of approximately 0.5.

3.1.3 Oxygenate selectivity as a function of various elementary rate constants. The effect of varying rate constants of methane formation on the selectivity of oxygenate formation is illustrated in Fig. 10–12.

Fig. 10 illustrates competition between methane selectivity and selectivity of oxygenate formation. The relative rate of methane formation is altered by changing the activation energies of the transformation of "CH_{ads}" to "$CH_{2,ads}$". This would correspond to a relative increase in the M–C bond energy for instance by an increase of surface metal atom coordinative unsaturation. The selectivity of oxygenate formation increases with increased methane selectivity. This is because chain growth through "CH_{ads}" insertion competes with termination through CO insertion.

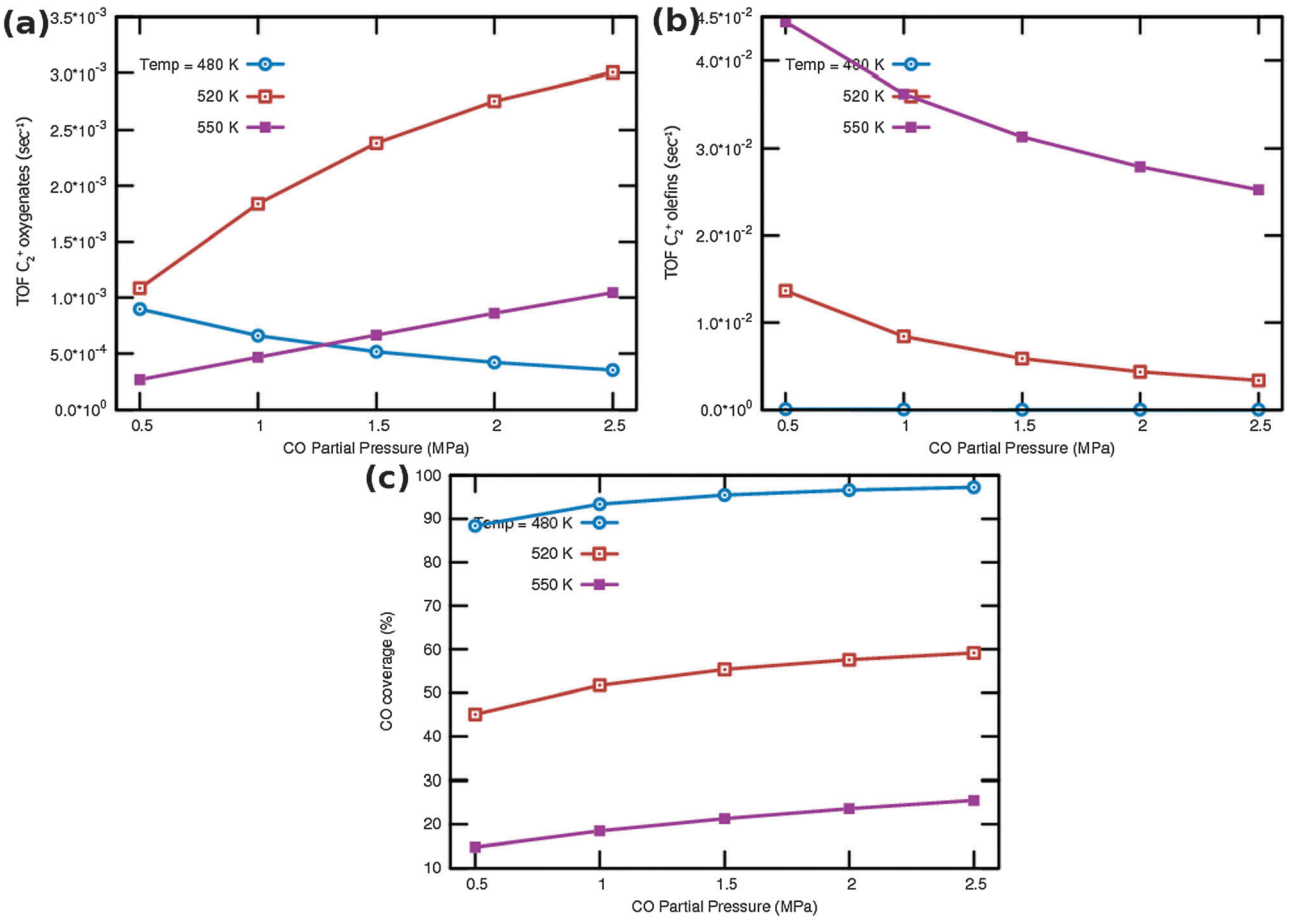

Fig. 9 C_{2+} (a) oxygenate and (b) olefin TOF (s^{-1}) as a function of CO partial pressures at three different temperatures. Also plotted in (c) is the CO surface coverage. H_2 partial pressure is maintained constant at 1.5 MPa.

Table 1 Steady state coverages (in ML) of the most dominantly present species at three different CO partial pressures corresponding to the results shown in Fig. 9. Three temperature ranges are shown in each case. 'Others' in the right hand most column shows the combined coverages of all other surface species other than those explicitly shown in other columns

Temp. (K)	CO	C	CH_2	CHCH	Vacancies	Others
p_{CO} = 0.5 Mpa						
480	0.8839	0.0025	0.0249	0.0786	0.0053	0.0048
520	0.4502	0.0466	0.0551	0.3925	0.0359	0.0197
550	0.1478	0.1602	0.0464	0.5515	0.0652	0.0289
p_{CO} = 1.5 Mpa						
480	0.9546	0.0009	0.0094	0.0313	0.0019	0.0019
520	0.5533	0.0285	0.0337	0.3591	0.0147	0.0107
550	0.2131	0.1148	0.0332	0.5886	0.0314	0.0189
p_{CO} = 1.5 Mpa						
480	0.9726	0.0006	0.0057	0.0188	0.0012	0.0011
520	0.5916	0.0223	0.0264	0.3423	0.0094	0.008
550	0.2552	0.0968	0.028	0.582	0.0225	0.0155

As a consequence chain growth parameter α decreases as can be observed from Fig. 10a.

A related effect is illustrated in Fig. 11. Now the activation barrier of the chain growth rate constant is varied. As in the previous case the selectivity of oxygenate formation is negatively affected when the chain growth rate constant is increased.

The selectivity of oxygenate formation is of course negatively affected when the olefin termination rate is increased (Fig. 12c). An increase of the rate constant of olefin termination will decrease α (Fig. 12a) and thus the selectivity of oxygenate formation. As a consequence the selectivity of methane formation (Fig. 12c) will increase.

Table 2 shows that the surface coverages are hardly affected by variation of the hydrocarbon termination rate. This is expected as long as there is no change in the rate controlling step, the interconversion of CO to surface "CH" species.

3.1.4. Summary. In the Fischer–Tropsch reaction the selectivity to produce long chain oxygenates *versus* olefins strongly depends on temperature and pressure. In agreement with experimental observations a low temperature and high partial pressure of CO[40] favour long chain oxygenate formation. Within the carbide mechanism increased oxygenate formation occurs at a cost of increased selectivity of methane formation. This is because CO insertion competes with "CH" insertion into the growing hydrocarbon chain. Low temperature experiments

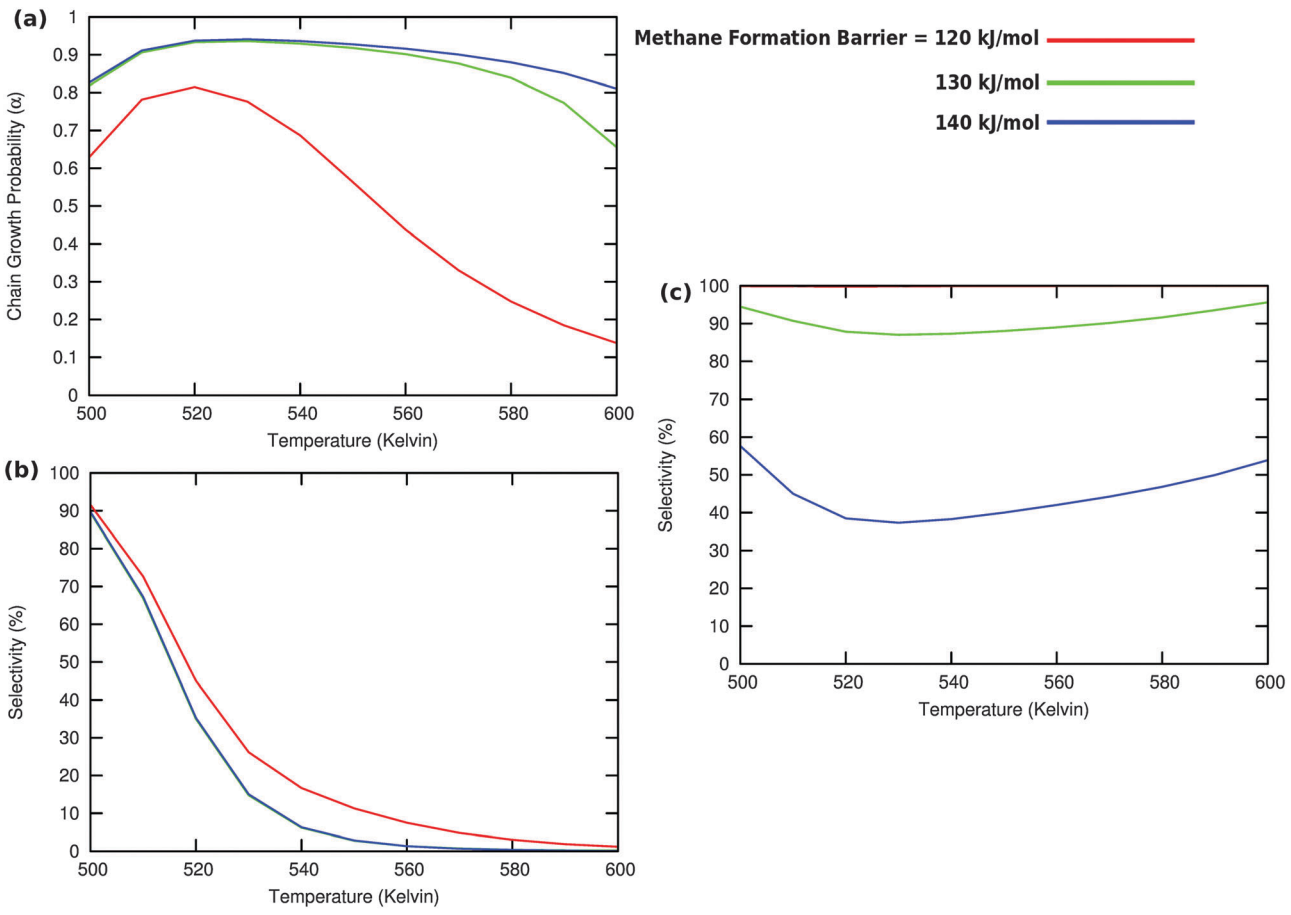

Fig. 10 (a) The chain growth probability α, (b) the oxygenate over olefins selectivity and (c) the methane over olefins selectivity as a function of temperature for different values of methane formation barriers. The CO activation barrier in each case is E_{act}^{CO} = 130 kJ mol^{-1}, the olefin termination activation energy change is $E_{act}^{(R-CH)\rightarrow(R-CH_2)} = 100$ kJ mol^{-1} and the change in activation energy for C–C coupling $E_{act}^{(R-H)\rightarrow(R-CH_2)} = 70$ kJ mol^{-1}. The CO pressure is maintained at p_{CO} = 0.5 MPa and the H_2 pressure is P_{H_2} = 1.5 MPa.

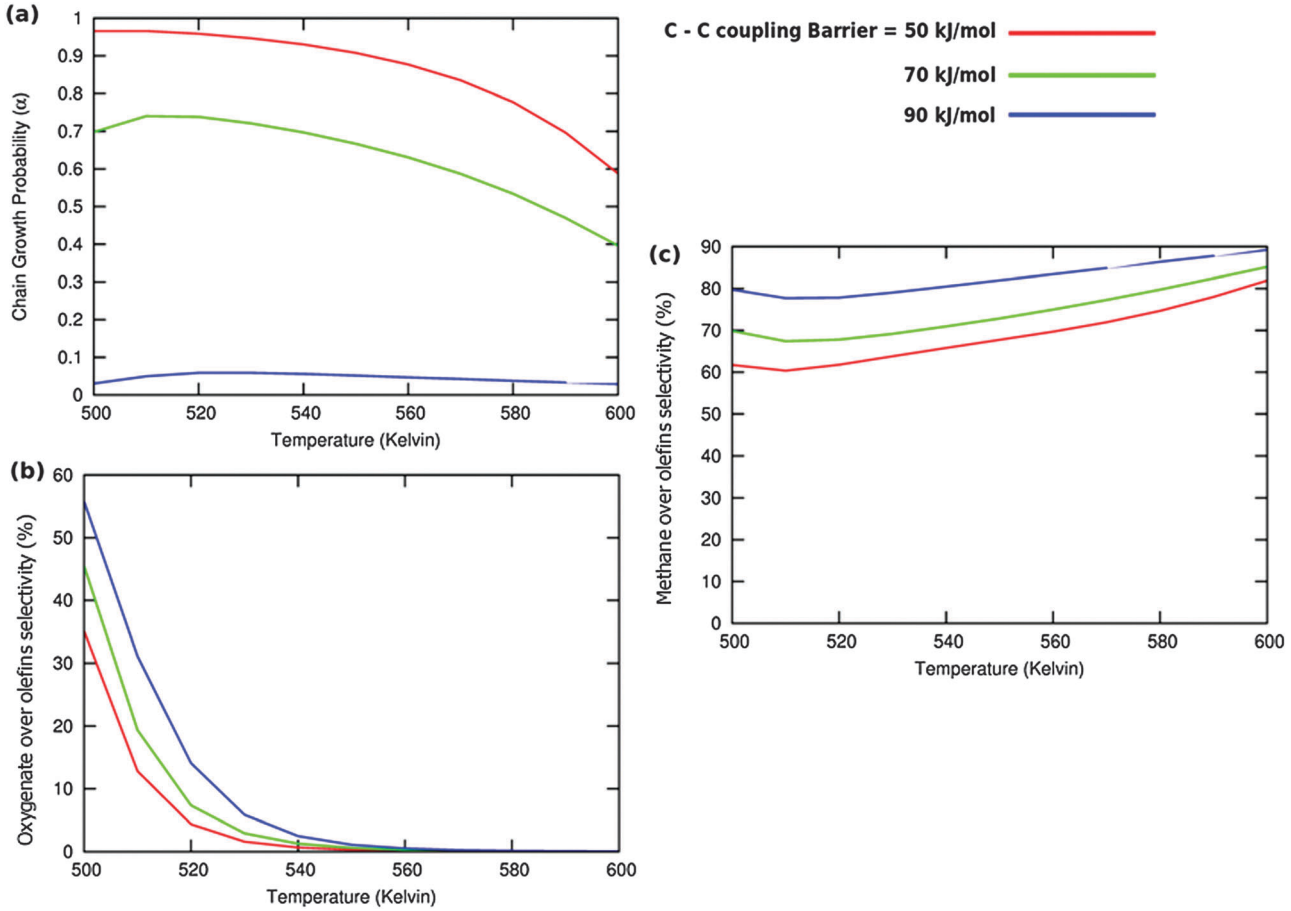

Fig. 11 (a) The chain growth probability (α), (b) the oxygenate over olefins selectivity and (c) the methane over olefins selectivity as a function of temperature for different values of C–C coupling barriers. The CO activation barrier in each case is E_{act}^{CO} = 130 kJ mol^{-1}, the olefin termination barrier is $E_{act}^{(R-CH)\rightarrow(R-CH_2)} = 100$ kJ mol^{-1} and the barrier for methane termination $E_{act}^{CH_2\rightarrow CH_3} = 130$ kJ mol^{-1}. The CO pressure is maintained at p_{CO} = 0.5 MPa and the H_2 pressure is P_{H_2} = 1.5 MPa.

with Ru nanoparticles[40] indicate that long chain oxygenate production is possible with a maximum CH_4 selectivity of 10%.

According to quantum-chemical calculations[21] the activation energy of CO insertion in the growing hydrocarbon chain is of the order of 50 kJ mol^{-1} and the overall activation energy to form the aldehyde is 90 kJ mol^{-1}. The overall reaction of the CO insertion reaction is endothermic by 60 J mol^{-1}. The CO insertion reaction competes with the chain growth reaction by insertion of a "CH" monomer into the growing hydrocarbon chain. The activation barrier for this reaction is of the order of 50–70 kJ mol^{-1}.

We have used activation energies of CO insertion into the growing hydrocarbon chain and formation of final products by successive hydrogen addition steps representative of values as found in the literature from quantum-chemical calculations typical for metals such as Co, Ru or Rh.[21]

We have varied the activation energies of some critical reaction steps in order to deduce chemical information to improve selectivity for long chain oxygenates.

When the activation energy for CO bond cleavage is low, the probability of long chain hydrocarbon formation is high. The relative rate of CO insertion is low because of its competition with CO dissociation. Hence there is an optimum in the chain growth probability *versus* oxygenate selectivity. The preference of Rh for oxygenate formation and also its limited yield of higher oxygenated hydrocarbons are due to its relatively increased barrier of CO dissociation with respect to Co and Ru.[35] The competition between oxygenate formation selectivity and chain growth probability becomes even more apparent when we discuss the chain growth mechanism through CO insertion in the next section.

3.2 Microkinetics according to the chain growth through the CO insertion mechanism

A high probability for chain growth requires that the rate of monomer insertion into the growing hydrocarbon chain is fast compared to the rate of the chain growth termination step. In the case of the carbide mechanism this implies the "CH" species that is inserted into the growing hydrocarbon chain is not rapidly removed as methane, but is rapidly inserted into the growing hydrocarbon chain. The monomer to be inserted into the growing hydrocarbon chain within the CO insertion chain growth mechanism is CO. A "C_2O" intermediate is formed by recombination of "CH_x" with CO. The higher hydrocarbons

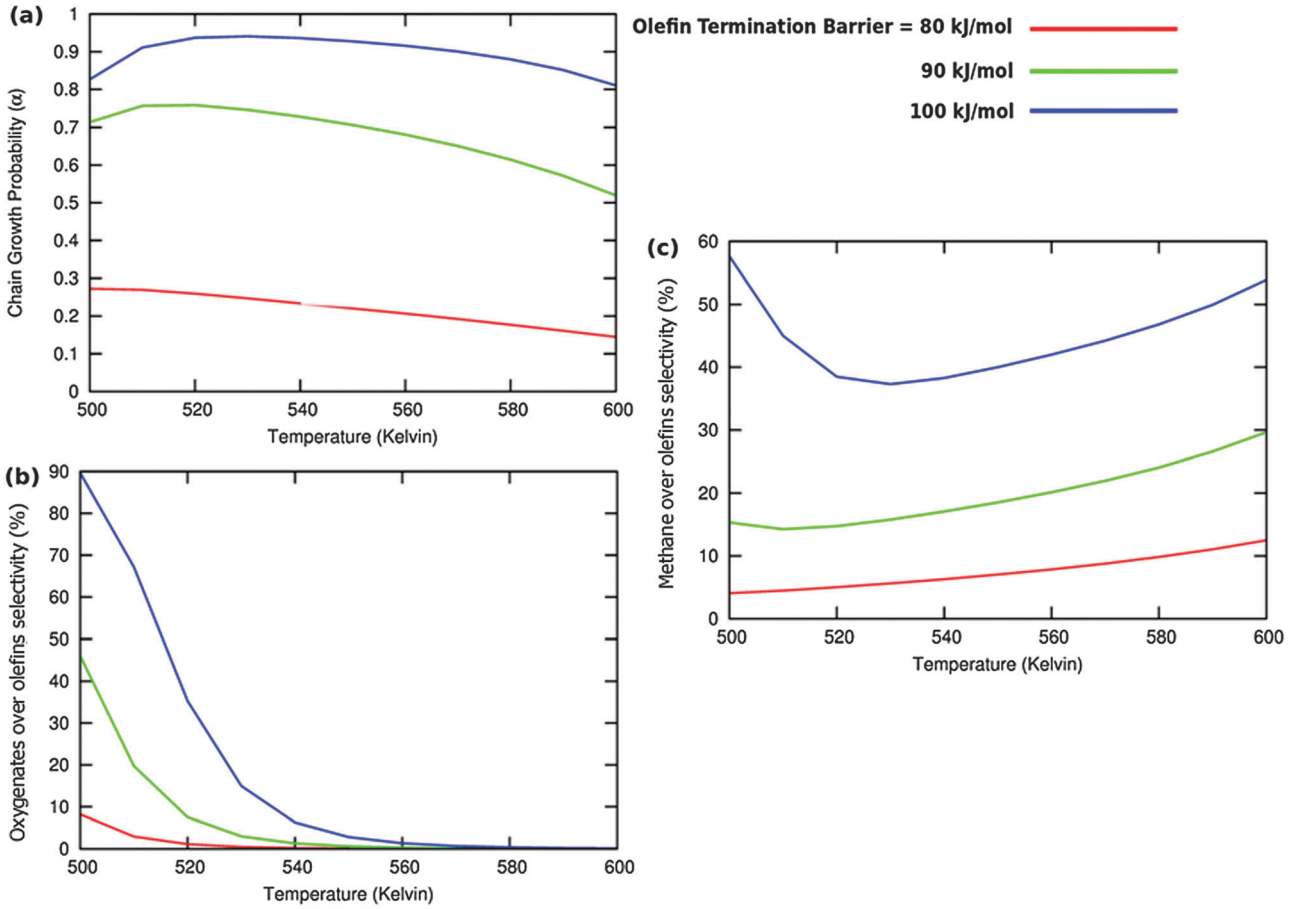

Fig. 12 (a) The chain growth probability α, (b) the oxygenate over olefins selectivity and (c) the methane over olefins selectivity as a function of temperature for different values of olefin termination barriers. The CO activation barrier in each case is E_{act}^{CO} = 130 kJ mol^{-1}, the C–C coupling barrier is $E_{act}^{(R-H)\rightarrow(R-CH_2)} = 70$ kJ mol^{-1} and the barrier for methane termination $E_{act}^{CH_2\rightarrow CH_3} = 140$ kJ mol^{-1}. The CO pressure is maintained at p_{CO} = 0.5 MPa and the H_2 pressure is P_{H_2} = 1.5 MPa.

Table 2 Steady state coverages (in ML) of the most dominantly present species as a function of different olefin termination barriers corresponding to the results shown in Fig. 12. Three temperature ranges are shown in each case. 'Others' in the right hand most column shows the combined coverages of all other surface species other than those explicitly shown in other columns

Olefin term. barrier (kJ mol^{-1})	CO	C	CH_2	CHCH	Vacancies	Others
Temp. = 480 K						
80	0.8876	0.0025	0.0244	0.0755	0.0053	0.0047
90	0.8696	0.0027	0.0266	0.0911	0.0052	0.0048
100	0.8681	0.0027	0.0267	0.0924	0.0052	0.0049
Temp. = 520 K						
80	0.4095	0.0469	0.0554	0.4365	0.0327	0.019
90	0.4074	0.0469	0.0554	0.4387	0.0325	0.0191
100	0.5403	0.0445	0.0526	0.2986	0.0431	0.0209
Temp. = 550 K						
80	0.1385	0.1576	0.0456	0.5692	0.0611	0.028
90	0.1188	0.1508	0.0437	0.6081	0.0524	0.0262
100	0.1749	0.1663	0.0481	0.5023	0.0772	0.0312

result from insertion of CO into "C_n" species that are generated by C–O bond cleavage of the "C_nO" intermediate. Since the "C_1" intermediate is only used to initiate the growing hydrocarbon chain, differently from the carbide chain growth mechanism, in this case high chain growth probability α_{CO} does not require relatively fast CO dissociation. Instead of expression eqn (1) for α according to the carbide mechanism, the coarse grained kinetics expression for chain growth α_{CO} becomes eqn (7):[21]

$$\alpha_{CO} = \frac{k_p\theta_v k_f\theta_{CO}}{(k_t^H + k_f\theta_{CO})(k_t'' + k_p\theta_v)} \quad (7)$$

Long chain growth catalysis requires k_p, the elementary rate for C–O bond cleavage in the "C_nO" intermediate, to be fast compared to k_t'', the elementary rate constant for chain growth termination with oxygenate as the product.[21] k_f is the rate constant of CO insertion into the growing hydrocarbon chain "C_n". θ_v is the vacancy surface concentration.

We have previously shown[21] that then available quantum-chemical data relevant to this mechanism give too slow apparent rate constants for chain growth (determined by k_p and k_f) compared to the rate constants of surface intermediate conversion to the product, k_t^H and k_t'', for the CO insertion chain growth mechanism to give high chain growth probabilities.

Recently it has been argued that the rate of chain growth within the CO insertion chain growth mechanism is underestimated in these microkinetics simulations because coverage dependent adsorbate–adsorbate interactions have been ignored.[18,41] Indeed as the microkinetics simulations of the previous section indicate under the Fischer–Tropsch conditions the surface can be considered highly covered with reaction intermediates.

One can implement the consequences of such adsorbate–adsorbate interactions in microkinetics simulations by using the corresponding calculated values of the activation energies of the elementary reaction rate constants and reaction intermediates in the simulations.[42] Generally one expects elementary association reactions to have reduced activation energies, but bond cleavage reactions to have increased activation energies.

We will present here microkinetics simulations based on reaction intermediate adsorption energies and rate constant activation energy values of the Saeys group[18] that represent the case of a highly covered Co(0001) surface. Their data have been used to construct the two micro-mechanistic models of the CO insertion chain growth model shown in Fig. 4a and b. Since in the two respective cases the carbonaceous intermediates that are generated have very different relative stabilities the corresponding reaction energy diagrams are quite different.

Results of the microkinetics simulations for the CO insertion chain growth reaction with high coverage are shown in Fig. 13.

Clearly no long chain hydrocarbons are formed, but C_2 formation is possible. In case (a) also a substantial amount of oxygenate is found. The results are consistent with many quantum-chemical results[22,43–47] that indicate that C_1 and CO recombination can occur with relatively low activation barriers.

This recombination is essentially different from subsequent insertions of CO in the adsorbed longer hydrocarbon chains that have higher activation energies.

Selective C_2 formation without methane formation is a technologically important reaction.[48]

Next to the apparent activation energies of the overall C–C bond formation reaction, the other parameter that determines chain growth probability is the rate constant k_t^H of the "C_n" intermediate termination that produces the olefin product.

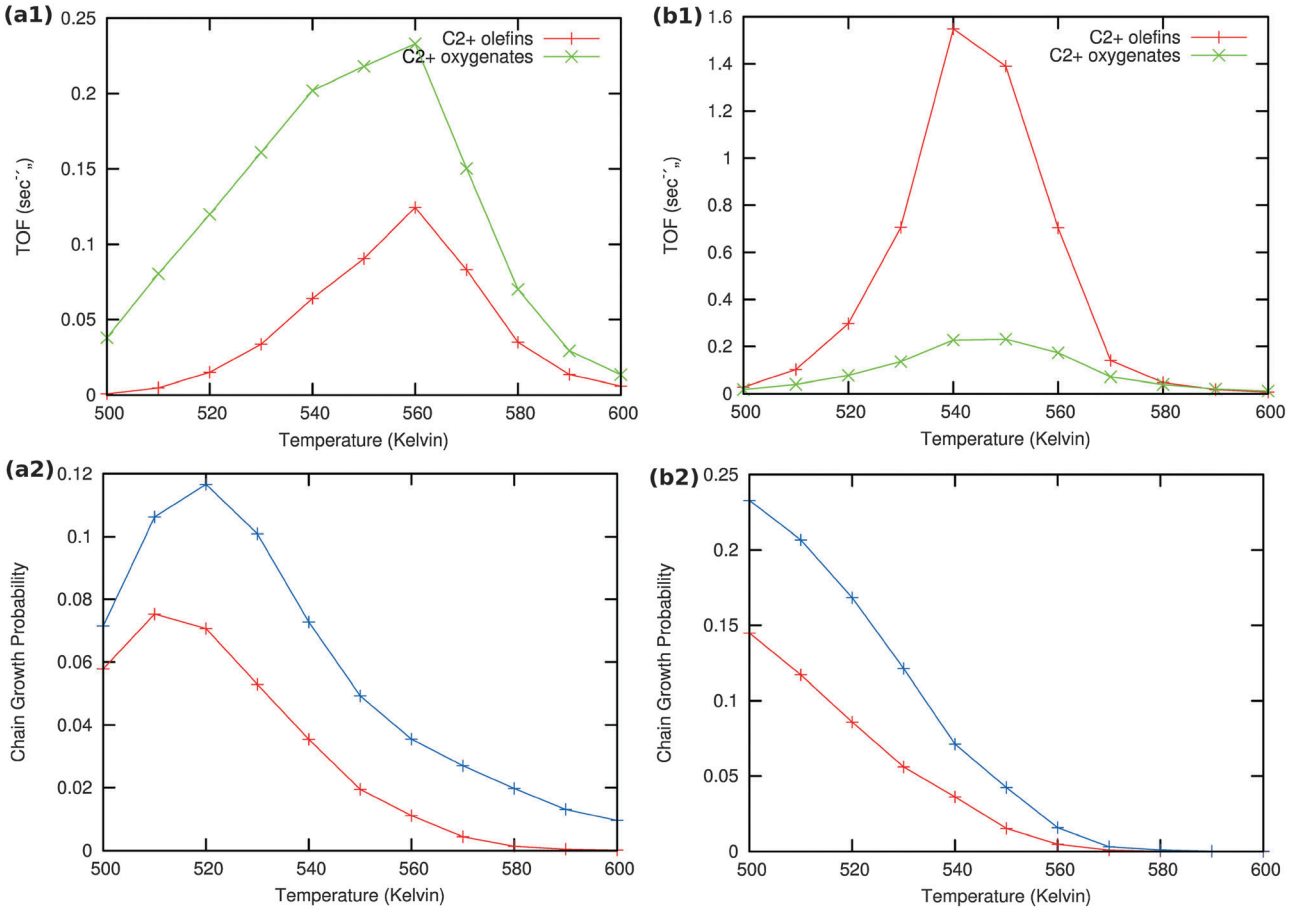

Fig. 13 Microkinetics results of the two mechanistic schemes depicted in Fig. 4a and b. Total TOFs and individual product yields are shown. Figures to the left (a1) & (a2) correspond to scheme in Fig. 4a and figures to the right (b1) & (b2) correspond to scheme 4b. In figure (a2) the red curve shows the chain growth probability (α) with the default rate constants given in Table S2 (ESI†), and blue curves show the chain growth probability (α) with a decreased rate constant of olefin desorption obtained by lowering the respective pre exponential values from 10^{16} to 10^{12}. In figure (b2) the red curve shows the chain growth probability (α) with the default rate constants given in Table S2 (ESI†), and blue curves show the chain growth probability (α) with a decreased rate constant of olefin desorption obtained by increasing the respective activation barriers from 70 kJ mol^{-1} to 100 kJ mol^{-1}.

In order to test the sensitivity of the results in Fig. 13(a2) and (b2) we have compared values of the chain growth probabilities for decreased values of the rate of desorption of the olefins. In case (a) the pre-exponential value of the olefin desorption rate has been decreased from 10^{16} to 10^{12}, in case (b) the activation barrier of olefin desorption rate has been increased from 70 kJ mol^{-1} to 100 kJ mol^{-1}.

As can be observed in the corresponding Fig. 13 the chain growth probabilities in both cases are slightly increased, but remain low. This confirms the conclusion that the CO insertion chain growth path mechanism will not lead to long chain hydrocarbon products.

The microkinetics results of this section and previous sections reveal that one has to be careful when concluding the validity of the CO insertion mechanism for chain growth based on arguments that relate to a relation between surface concentration and transient kinetics as recently done by Kruse *et al.*[49] It can be clearly seen also from the simulations presented in Section 3.1, that a high surface concentration of CO can be consistent with the carbide mechanism and is no proof of the CO insertion chain growth mechanism. This is consistent with the elegant demonstration by *in situ* PM-RAIRS experiments by Beitel *et al.*[50,51] that CO adsorbed to step edges is consumed during Fischer–Tropsch reaction, which illustrates that it is replaced by different species. We observe from our simulations that within the carbide mechanism CO is replaced by growing adsorbed hydrocarbons. Previously published quantum-chemical calculations of the chain growth at the stepped Ru(1121) surface[52] have shown that at the step-edges C atoms generated by CO dissociation upon addition of a hydrogen atom move from their four-fold adsorbed position within the step to three-fold position at the step-edge, which is also the site of the chain growth reaction. The movement of the C atom away from the internal part of the step to its edge prevents deactivation of the step site.

We have reviewed elsewhere[13] the very elegant early isotope labeling experiments by Biloen and Sachtler[10] and the work of Brady and Pettit[53,54] and of Maitlis,[55,56] which provide strong experimental support for the carbide chain growth reaction path.

4. Conclusion: comparison of theory and experiment

In this section we will discuss the critical rate parameter relations that determine the selectivity of long chain oxygenate formation and we will relate this with available experimental results. For a comparison with experimental results we will mainly base ourselves on material reviewed in papers.[4,5]

Direct comparison of the microkinetics simulations as presented here with experimental data of practical catalysts with often complex composition will have to remain speculative. We will therefore limit the discussion to a general comparison of trends in catalyst performance data with the microkinetics simulations results. Since we will mainly compare with experiments that concern alcohol production, we will consider the alcohols to be rapidly formed by consecutive hydrogenation once the aldehyde is produced as the primary product.

Most of the experimental Fischer–Tropsch catalyst studies on oxygenate formation are based on Rh, Fe (carbide), Co, MoC_2 or MoS_2. When not modified by added promoting components such as alkali metals or additional transition metals, these materials produce only alkanes or alkenes except when Rh and Fe catalyst materials are used. We earlier referred to nanoparticle Ru catalysts[40] that also produce long chain oxygenates, but only in a very low temperature regime where syngas conversion has a low turnover frequency.

Promotion substantially increases the oxygenate production of most of the catalysts, but oxygenate *versus* hydrocarbon selectivity rarely exceeds 50% (the catalysts of highest selectivity are Rh/ZrO_2 or Rh/TiO_2) and is usually substantially less. Interesting with respect to the microkinetics simulation results of Section 3.2 is that C_1 and C_2 oxygenate production is usually far in excess of that of C_3^+ oxygenates, except for MoC_2 or MoS_2 based systems, where it may become comparable. Clearly there is a significant scope for improvement.

According to the microkinetics simulations the relatively high overall barrier for C–C bond formation by the CO insertion chain growth mechanism makes this reaction route unsuitable for long hydrocarbon formation. One has to note however that the mechanism of C_2H_4O formation is similar to that in the carbide chain growth route.

Within the carbide mechanism the relatively low activation energy of the rate of chain growth and relatively high activation energy for CO insertion into the adsorbed growing hydrocarbon chain are consistent with the possibility of long chain oxygenate formation.

Long chain oxygenate product formation competes with the following reactions:

(a) methane (methanol) formation

(b) recombination of "CH_x" with another "CH_x" that produces ethylene or "C_nH_y" with another "CH_x" ($n > 1$) that produces alkene. These recombination steps are to be compared with reaction of CO_{ads} with "CH_x" or "C_nH_y"

(c) decomposition of "CH_xCO" or "C_nH_yCO" into "CH_xC" or "C_nH_yC" and "O_{ads}".

Ad (a)

The rate of methane formation depends on the relative rate of C–O bond cleavage to give "CH_x" *versus* the rate of "CH_x" hydrogenation to methane. Within the carbide mechanism methane formation from "CH_x", the building unit of the chain growth reaction, competes with the rate of incorporation of "CH_x" into the adsorbed growing hydrocarbon chain.

We have studied in Section 3.1.1 the sensitivity of catalyst performance with respect to the activation barrier for C–O bond activation. As long as the CO activation barrier is low, as is the case on stepped reactive surfaces, the chain growth probability does not depend on the activation energy of C–O bond cleavage. The rate of CO consumption as well as chain growth probability is then controlled by the rate constant of chain growth termination.[12] This we have called preciously the Fischer–Tropsch

chain growth kinetics limit case. Then the reactive catalyst center becomes covered with mainly hydrocarbon intermediates.

When the activation energy of C–O bond activation increases, for instance when a more reactive metal such as Ru is replaced by Co or a less reactive surface is chosen with different step-edges, the CO consumption rate and chain growth probability can become limited by the rate of "CH_x" production. Then the rate of CO consumption becomes controlled by the elementary rate constant of C–O bond cleavage. This kinetics limit we have previously identified as the monomer formation kinetics limit.[12] It is in this kinetics regime that most Fischer–Tropsch catalysts operate.[13]

When the activation energy of CO activation increases further, the route towards C–O bond cleavage starts to compete with that of the hydrogen activated bond cleavage reaction. This is typically the situation for CO activation on the dense surfaces of Co, Rh or Ru or metal surfaces of low reactivity as for Ni.[26] Recently Salmeron *et al.*[57] have demonstrated hydrogen activated C–O bond cleavage on nanoparticles of Co.

Clearly direct CO activation to give "CH_x" as well as hydrogen activated C–O bond cleavage contain hydrogen atom addition as an important step, so that kinetically the difference between the two is not essential but the apparent activation energy to produce CH_x. We have found that on the reactive Rh(211) surface[58] both reaction paths have the same apparent activation energies.

To produce oxygenate the rate of CO bond cleavage has to be reduced. C–O bond cleavage and CO insertion into "CH_x" or longer adsorbed hydrocarbon fragments are competing reactions and will also compete with methanol formation.

Ad (b)

To produce long chain oxygenates we find that the overall activation barrier of C–O bond cleavage of the CO to "CH_x" transformation reaction should not be too low, since otherwise competition with CO insertion into the growing hydrocarbon chain becomes too unfavourable. On the other hand the activation energy of CO activation should not be too high, otherwise no "CH_x" species will be generated to be inserted into the growing hydrocarbon chain. Then "CH_x" will be mainly converted into methane. In the extreme case of a very high activation energy of CO activation methanol will be formed, as for instance on the Cu methanol catalyst.[59]

On Ni the rate of CO activation is too low,[60] which makes it the preferred catalyst for methane formation. In order to compete with methane formation the upper bound to the activation energy of C–O bond cleavage has to be between 90 and 120 kJ mol^{-1}, dependent on the reactivity of the metal surface to hydrogenate surface "CH_x" intermediates to methane. On dense surfaces that have a low M–C interaction energy the lower value applies, on the more open reactive surfaces the higher value.

The lower bound for the activation barrier of C–O bond cleavage due to competition with the activation energy of CO insertion into the growing hydrocarbon chain to give the aldehyde is of the order of 90 kJ mol^{-1}. It is consistent with a high chain growth probability because within the carbide mechanism the apparent activation energies for C–C bond formation are in the regime between 50 and 70 kJ mol^{-1}.

The lower bound to the activation energy of C–O bond activation implies that the reactive stepped Ru surfaces are no suitable catalysts for oxygenate formation. This conclusion agrees with experiment[40] that indicates that only small nanoparticles, which may be expected to have a low concentration of step-edge sites,[61] show high long chain oxygenate selectivity at low temperature, but with a very low CO consumption rate. Because of the increased CO activation barrier at a higher temperature less reactive Rh shows a higher oxygenate formation selectivity. A high selectivity can be maintained with acceptable turnover frequencies, however at a cost of longer chain oxygenates.

Alloys that combine a metal that binds CO strongly but does not activate C–O bond cleavage, such as Ir, with a metal that dissociates CO with an activation energy, such as Co have been demonstrated to show significant selectivity towards formation of C_2 oxygenates, with minor coproduction of methanol.[5]

The additional condition that has to be satisfied in order to obtain long chain oxygenates is that termination through CO insertion is favourable compared to termination as alkene.

The quantum-chemistry of CO insertion has been studied extensively within the context of hydroformulation.[62] The availability of empty d-valence electron states of surface metals atoms of low energy that reduce repulsive interaction between the lone pair electrons of CO and the occupied C atoms of the reacting adsorbed hydrocarbon intermediate by electron donation to the metal atoms reduces the CO insertion barrier. Also Lewis acid activation of CO[63] lowers the activation energy of C–O bond cleavage. Possibly for these reasons addition of reducible metal oxide catalysts as vanadium or Mn oxides to Rh shows significantly enhanced yields of oxygenate formation.[63]

From scaling law arguments[64] it is known that the activation energies for hydrogen transfer reaction increase with an increase of the surface metal M–C bond energy. Since the intermediate to be hydrogenated to the olefin is an alkenyl or alkylidyne intermediate, to which a hydrogen atom has to be added[13] a stronger M–C bond will reduce the rate of hydrocarbon formation since the rate constant of chain growth termination will be decreased.

A larger M–C bond interaction will not only decrease the rate constant of methane formation, but also decrease the rate of C–C bond formation compared to that of CO insertion. This is possibly the reason that promoted MoC_2 or MoS_2 based catalysts have been reported[5] to produce the highest fraction of linear C_3^+ oxygenates.

Ad (c)

Rh catalysts have been experimentally[4,5] as well computationally[21] most extensively investigated with respect to oxygenate formation. We have shown in Section 3.2 that according to the data of Saeys *et al.*[18] on Co, CO insertion into adsorbed CH proceeds with a relatively low barrier and that because of the ease of cleavage of the C–O bond the main reaction product according to this reaction path is ethylene. Computational quantum-chemical data of comparable elementary reaction steps for C_2 oxygenate

formation on different surfaces of Rh[22] summarized in ref. 20 and Ru surfaces[13] are also available. They indicate that the recombination reaction of CO_{ads} and "CH_{ads}" will readily occur on Rh, but show a higher activation energy barrier on Ru.[13] On Rh activation of the C–O bond of inserted CO has a substantially higher barrier than on Ru. Whereas the relative rate of methane formation from adsorbed "CH_x" is faster on Rh than Ru (the M–C bond is stronger on the latter), Rh CO insertion into CH_x will more favourably compete with "CH_x" recombination and the rate of bond cleavage of C═O will be suppressed.[37]

Since of the three metals considered more reactive Ru has the stronger M–C bond the observation of low temperature long chain oxygenate formation is consistent with the theoretical considerations. At higher temperatures Rh should be the better catalyst for shorter chain oxygenates.

Takeuchi *et al.*[32] found that highly dispersed Co catalysts that are Sr promoted show enhanced production of C_2 oxygenates compared to prediction according to the ASF product distribution plot. But for hydrocarbon formation ethylene production is suppressed. It is suggested by Spivey *et al.*[4] that this demonstrates preferred CO insertion into "CH_x". The recent observation by Galvis *et al.*[48] that at high temperature nanosized carbided Fe particles promoted by S and alkali are selective ethylene and propylene catalysts suggests that they are also produced through recombination of a "CH_{ads}" and CO_{ads} species. More reactive Fe compared to Co now rapidly catalyses C–O bond cleavage after the CO insertion reaction.

To conclude we will address the question whether significant improvements of the production of linear long chain oxygenates by further adaptation of Fischer–Tropsch catalysis may be expected.

The low temperature nanoparticle Ru catalyzed reaction[21] illustrates that a high chain growth oxygenate probability is possible. But the CO consumption rate is too low to be of practical interest.

Important at the low temperature are the low relative overall rate constants of methane formation and CO insertion *versus* the overall rate constant of chain growth through CH_x insertion.

A strong M–C bond will be beneficial since it will suppress methane formation, except that it will slow down C–C bond formation, which becomes endothermic when the M–C bond becomes too strong.[20]

The increased M–C bond energy will also lower the activation energy of C–O bond activation. Oxygenate formation is maximum when the rate constant of C–O bond activation of CO is approximately equal to the rate constant of the oxygenate termination reaction.[21]

Whereas this will be beneficial to the chain growth reaction it will decrease the oxygenate yield. The choice of a reaction center that is less electronegative will be beneficial, since a decrease of the M–O bond energy will decrease the elementary rate constants of CO activation and favour oxygenate formation.

As shown by Arakawa *et al.*[33,65] a small metal particle size will enhance the probability of oxygenate formation. On a small metal particle CO dissociation will have a low rate, but also the rate constant of chain growth, so primarily C_2 oxygenates can be expected.

The resulting conflicting dependencies on surface reactivity imply an optimum in oxygenate selectivity and the CO consumption rate, which not necessarily has to coincide. This is confirmed by experiments with promoted Rh catalysts,[4] that give maximum oxygenate yield for the vanadium promoted catalyst, but maximum selectivity of the TiO_2 promoted catalyst.

A computational study by Jenness *et al.*[66] indicates that reducible oxides promote a small charge deficit on the small Rh particles that enhances the M–C interaction energy and reduces the interaction with oxygen. This appears to agree with experimental data on vanadium promoted Rh catalysts[67,68] that show decreased methane formation due to an increased M–C interaction.

The complex catalyst formulations developed so far lack optimum catalyst performance, due to excess hydrocarbon formation. Whereas further improvement of long chain oxygenate formation through Fischer–Tropsch type catalysis is unlikely, improvements in selectivity and yield of C_2 oxygenates should be possible.

References

1 R. B. Anderson, H. Kölbel and M. Rálek, *The Fischer–Tropsch Synthesis*, Academic Press, 1984.
2 *Fischer–Tropsch Technology*, ed. A. P. Steynberg and M. E. Dry, Elsevier, Amsterdam, 2004.
3 H. H. Storch, N. Golumbic and R. B. Anderson, *The Fischer–Tropsch and Related Syntheses*, Wiley, New York, 1951.
4 A. Egbebia and J. J. Spivey, *Chem. Soc. Rev.*, 2007, **36**, 1514–1528.
5 S. K. Gangwal and V. Subramani, *J. Phys. Chem.*, 1986, **90**, 4752–4758.
6 E. B. M. Doesburg, X. Xiaoding and J. J. F. Scholten, *Catal. Today*, 1987, **2**, 125–170.
7 T. Fukushima, M. Ichikawa, T. Yokohama, N. Kosugi and H. Kurodan, *J. Phys. Chem.*, 1986, **90**, 1222–1224.
8 V. Ponec, *Studies in Surface Science and Catalysis*, 1991, p. 64.
9 I. M. Ciobîcă, R. A. van Santen, E. van Steen and M. M. Ghouri, in *Advances in Catalysis*, ed. H. Knozinger, B. C. Gates, Academic Press, 2011, vol. 54, pp. 127–187.
10 P. Biloen and W. M. H. Sachtler, *Adv. Catal.*, 1981, **30**, 165–216.
11 H. Pichler and H. Schulz, *Chem. Ing. Tech.*, 1970, **42**, 1162–1174.
12 R. A. van Santen, A. J. Markvoort, M. M. Ghouri, P. A. J. Hilbers and E. J. M. Hensen, *J. Phys. Chem. C*, 2013, **117**, 4488–4504.
13 R. A. van Santen, A. Markvoort, I. A. W. Filot, M. M. Ghouri and E. J. M. Hensen, *Phys. Chem. Chem. Phys.*, 2013, **15**, 17038–17063.
14 H. Schulz, in *Catalysis: From Principles to Applications*, ed. M. Beller, A. Renken and R. A. van Santen, Wiley-VCH, Weinheim, 2012.
15 S. Storsaeter, D. Chen and A. Holmen, *Surf. Sci.*, 2006, **600**, 2051–2063.

16 H. Kölbel, R. B. Anderson and M. Rálek, *The Fischer–Tropsch Synthesis*, Academic Press, 1984.
17 P. Hu, J. Cheng, P. Ellis, S. French, G. Kelly and C. M. Lok, *J. Phys. Chem. C*, 2008, **112**, 1308–1311.
18 M. Zhuo, A. Borgna and M. Saeys, *J. Catal.*, 2013, **297**, 217–226.
19 I. M. Ciobîcă, G. J. Kramer, Q. Ge, M. Neurock and R. A. van Santen, *J. Catal.*, 2002, **212**, 136–144.
20 A. J. Markvoort, R. A. Van Santen, P. A. J. Hilbers and E. J. M. Hensen, *Angew. Chem., Int. Ed.*, 2012, **51**, 9015–9019.
21 R. A. van Santen and A. Markvoort, *ChemCatChem*, 2013, **5**, 3384–3397.
22 N. Kapur, J. Hyun, B. Shan, J. B. Nicholas and K. Cho, *J. Phys. Chem. C*, 2010, **114**, 10171–10182.
23 O. R. Inderwildi, S. J. Jenkins and D. A. King, *J. Phys. Chem. C*, 2008, **112**, 1305–1307.
24 J. W. Mirwald and O. R. Inderwildi, *Phys. Chem. Chem. Phys.*, 2012, **14**, 7028–7031.
25 M. Ojeda, R. Nabar, A. U. Nilekar, A. Ishikawa, M. Mavrikakis and E. Iglesia, *J. Catal.*, 2010, **272**, 287–297.
26 S. Shetty, A. P. J. Jansen and R. A. van Santen, *J. Am. Chem. Soc.*, 2009, **131**, 12874–12875.
27 I. M. Ciobîcă and R. A. van Santen, *J. Phys. Chem. B*, 2003, **107**, 3808–3812.
28 R. A. van Santen, I. M. Ciobîcă, E. van Steen and M. M. Ghouri, in *Advances in Catalysis*, ed. B. C. Gates and H. Knozinger, Academic Press, 2011, ch. 3, vol. 54, pp. 127–187.
29 J. Yang, J. M. G. Carballo, A. Holmen, S. García-Rodríguez, S. Rojas, M. Odeja and J. L. G. Fierro, *J. Catal.*, 2011, **284**, 102–108.
30 P. B. Radestake, J. P. Den Breejen, G. L. Bezemer, J. H. Bitter, V. Frøseth, A. Holmen and K. P. de Jong, *J. Am. Chem. Soc.*, 2009, **131**, 7197–7203.
31 J. H. Bitter, G. L. Bezemer, H. P. C. E. Kuipers, H. Oosterbeek, J. E. Holewijn, X. Xu, F. Kapteijn, A. K. van Dillen and K. P. de Jong, *J. Am. Chem. Soc.*, 2006, **128**, 3956–3964.
32 K. Takeuchi, H. Arakawa, T. Matsuzaki and Y. Sugi, *Chem. Lett.*, 1984, **13**, 1607.
33 H. Arakawa, T. Hanaoka, T. Matsuzaki, Y. Sugi, K. Kanno and Y. Abe, *Catal. Today*, 2000, **58**, 271–280.
34 M. Neurock and R. A. van Santen, *Molecular Heterogenous Catalysis*, Wiley-VCH, 2006.
35 Z.-P. Liu and J. Chen, *J. Am. Chem. Soc.*, 2008, **130**, 7929–7937.
36 C. H. Bartholomew and R. J. Farrauto, *Fundamentals of Industrial Catalytic Processes*, Wiley, Hoboken, New Jersey, 2nd edn, 2005.
37 M. C. Valero and P. Raybaud, *Catal. Lett.*, 2013, **143**, 1–17.
38 I. M. Ciobîcă and R. A. van Santen, *J. Phys. Chem. B*, 2002, **106**, 6200–6205.
39 I. M. Ciobîcă, F. Frechard, R. A. van Santen, A. W. Kleyn and J. Hafner, *Chem. Phys. Lett.*, 1999, **311**, 185–192.
40 Y. Guan, X. Y. Quek, R. A. van Santen and E. J. M. Hensen, *ChemCatChem*, 2011, **3**, 1735–1738.
41 B. T. Loveless, C. Buda, M. Neurock and E. Iglesia, *J. Am. Chem. Soc.*, 2013, **135**, 6107–6121.
42 J. W. Niemantsverdriet and R. A. van Santen, *Chemical Kinetics and Catalysis*, Plenum Press, 1995.
43 J. Cheng, X.-Q. Gong, P. Hu, C. M. Lok, P. Ellis and S. French, *J. Catal.*, 2008, **254**, 285–295.
44 Y. Choi and P. Liu, *J. Am. Chem. Soc.*, 2009, **131**, 13054–13061.
45 Y.-H. Zhao, K. Sun, X. Ma, J. Liu, D. Sun, H.-Y. Su and W.-X. Li, *Angew. Chem., Int. Ed.*, 2011, **50**, 5335–5338.
46 M. Zhuo, K. F. Tan, A. Borgna and M. Saeys, *J. Phys. Chem. C*, 2009, **113**, 8357–8365.
47 D.-B. Cao, Y.-W. Li, J. Wang and H. Jiao, *J. Mol. Catal. A: Chem.*, 2011, **346**, 55–69.
48 H. M. T. Galvis, J. H. Bitter, C. B. Khare, M. Ruitenbeek, A. I. Dugulan and K. P. de Jong, *Science*, 2012, **335**, 835–838.
49 A. Bundhoo, J. Schweicher, A. Frennet, N. Kruse, D. Helen and F. Meunier, *J. Phys. Chem. C*, 2010, **114**, 2248–2255.
50 A. Laskov, G. A. Beitel, H. Oosterbeek and E. W. Kuipers, *J. Phys. Chem.*, 1996, **100**, 12494–12502.
51 C. P. M. de Groot, G. A. Beitel, H. Oosterbeek and J. H. Wilson, *J. Phys. Chem. B*, 1997, **101**, 4035–4043.
52 I. M. Ciobîcă, S. Shetty, E. J. M. Hensen and R. A. van Santen, *Chem. Commun.*, 2011, **47**, 9822–9824.
53 R. Pettit and R. C. Brady III, *J. Am. Chem. Soc.*, 1981, **103**, 1287–1289.
54 R. Pettit and R. C. Brady III, *J. Am. Chem. Soc.*, 1981, **102**, 6181–6182.
55 R. Quyoum, P. M. Maitlis, H. C. Long and M. L. Turner, *Appl. Catal., A*, 1999, **186**, 363–374.
56 P. M. Maitlis and V. Zanotti, *Catal. Lett.*, 2007, **122**, 80–83.
57 S. Carenco, A. Tuxen, M. Chintapalli, C.-H. Chuang, C. Escudero, E. Pach, P. Jiang, F. Borondics, B. Beberwyck, A. P. Alivisatos, G. Thornton, W.-F. Pong, J. Guo, R. Perez, F. Besenbacher and M. Salmeron, *J. Am. Chem. Soc.*, 2013, **135**, 2273–2278.
58 P. W. van Grootel, T. Zhu, I. A. W. Filot, S.-G. Sun, R. A. van Santen and E. J. M. Hensen, *J. Catal.*, 2013, **297**, 227–235.
59 S. Lee, *Methanol Synthesis Technology*, CRC Press, 1989.
60 F. Abild-Pedersen, M. P. Andersson, I. N. Remediakis, T. Bligaard, G. Jones, J. Engbæk, O. Lytken, S. Horch, J. H. Nielsen, J. Sehested, J. R. Rostrup-Nielsen, J. K. Nørskov and I. Chorkendorff, *J. Catal.*, 2008, **255**, 6–12.
61 A. Hellman, K. Honkala, I. N. Remediakis, A. Logadottir, A. Carlsson, S. Dahl, C. H. Christensen and J. K. Nørskov, *Science*, 2005, **307**, 555–558.
62 R. Hoffman and D. L. Thorn, *J. Am. Chem. Soc.*, 1978, **100**, 2079–2090.
63 M. Ichikawa and W. M. H. Sachtler, *J. Phys. Chem.*, 1986, **90**, 4752–4758.
64 J. Greely, F. Abild-Pedersen, F. Studt, J. Rossmeisl, T. R. Munter, P. G. Moses, E. Skúlason, T. Bligaard and J. K. Nørskov, *Phys. Rev. Lett.*, 2007, **99**, 016105.
65 K. Takeuchi, H. Arakawa, T. Matsuzaki and Y. Sugi, *Chem. Lett.*, 1985, 1315–1318.
66 J. R. Schmidt and G. R. Jenness, *ACS Catal.*, 2013, **3**, 2881–2890.
67 R. A. van Santen and T. Koerts, *Catal. Lett.*, 1990, **6**, 49–57.
68 R. A. van Santen and T. Koerts, *J. Catal.*, 1992, **134**, 12–23.

